Supplementary Materials for Chen et al

- Fig. S1. Analyses of EL7E1 immuno-purified Rad53.
- Fig. S2. Rad53 phosphorylation analyses upon S phase DNA damage.
- Fig. S3. Examination of Mrc1- and Rad9-mediated Rad53 activation.
- Fig. S4. Combined effects of *rad9*Δ or *mrc1*Δ with SCD1 mutations on Rad53 auto-activating and priming phosphorylation.
- Fig. S5. Combined effects of *rad9*Δ with FHA mutations on phosphorylation dependent depletion of unphosphorylated SCD1 fragment.
- Table S1. Genotypes of yeast strains used in this study.
- Table S2 (Excel dataset). List of all detected Rad53 tryptic fragments and the quantitation by MAXQUANT for their unlabeled and SILAC-labeled counterparts from 5 independent biological replicates of WT sample after S phase MMS treatment.
- Table S3 (Excel dataset). Rad53 phosphorylation sites identified in this study by MAXQUANT analysis in 5 independent biological replicates of EL7E1-immuno-putified WT Rad53 after S phase MMS treatment.
- Table S4 (Excel dataset). Mrc1 phosphorylation sites identified in this study by MAXQUNANT analysis.
- Table S5 (PDF file). All annotated, mass labeled spectra for Tables S2-4.

Supplementary Figures Legends

Figure S1. Analyses of EL7E1 immuno-purified Rad53.

(A) Western blot analysis of cell lysates before and after EL7E1 immunoprecipitation under unperturbed (-) and MMS-treated (+) conditions, showing the protein levels and characteristic mobility shifts of Rad53. Aliquots of eluents after immunoprecipitation were examined on the same blot.

(B) Coomassie blue staining for the indicated unlabeled and spiked-in SILAC-labeled EL7E1 immuno-purified Rad53 protein complexes. Tryptic peptides from 12 gel slices per mixed sample were subjected to LC-MS/MS analysis using an LTQ-Orbitrap hybrid MS analyzer. The majority of Rad53 was contained in fraction 4.

Figure S2. Rad53 phosphorylation analyses upon S phase DNA damage.

(A, B) Bar graphs indicating the effects of mutations of the kinase domain or checkpoint mediators on the relative levels of mono-phosphorylated S789, S793 or S795, di-phosphorylated S789-S793, S789-S795, or S793-S795, and tri-phosphorylated S789-S793-S795 (A), and phosphorylated S198, S373, S750, S766, and S789 (B). Note that the detection of phosphorylation at S789, S793, and S795 was resulted from the same tryptic Rad53 fragment IHS^{789}VSLS^{793}QS^{795}QIDPSK so that, compared to WT, impairment of phosphorylation at S789, but not S793 and S795, in kinase-defective strains would cause a pattern of impairment for the levels of mono-phosphorylated S789, di-phosphorylated S789-S793/S789-S795, and tri-phosphorylated S789-S793-S795 but enhancement for the levels of mono-phosphorylated S793/S795 and di-phosphorylated S793-S795.

(C) Precursor mass spectral scans of the unlabeled (light) and spiked-in SILAC-labeled (heavy)

Rad53 tryptic fragment counterparts for an unmodified Rad53$^{670-679}$ fragment FLLQDGEDIK as input control (a) and the unphosphorylated (b) and mono-, di-, tri-, and tetra-phosphorylated (c-f, respectively) SCD2 Rad53$^{468-492}$ fragment MSPLGSQSYGDFSQISLSQSLSQQK (the M468 was S-oxidized) in the indicated strains. Mass to charge ratio (m/z) of the monoisotopic precursor is labeled in each top panel.

(D) Tandem mass spectral assignments of a tetra-phosphorylated SCD1 tryptic peptide [the N-terminal Met is N-acetylated and S-oxidized in the monoisotopic precursor m/z of 1170.41 $(MH_2)^{2+}$]. * indicates the signature loss of phosphoric acid (98; H_3PO_4) that is labeled in the b and y ion assignments.

(E) Tandem mass spectral assignments of a tetra-phosphorylated SCD2 tryptic peptide [the Met is S-oxidized in the mono-isotopic precursor m/z of 1013.72 $(MH_3)^{3+}$]. * indicates the signature loss of phosphoric acid (98; H_3PO_4) labeled in the b and y ion assignments.

(F) Bar graphs showing the estimated phospho-stoichiometries of selected Mec1/Tel1-target sites (a) and auto-phosphorylation sites (b) based on the relative depletion ratios of the corresponding unphosphorylated peptides. Note that S789 and S791 in (a) and S175, S743, and S750 in (b) with small font are not Mec1/Tel1 sites and auto-phosphorylation sites, respectively.

Figure S3. Examination of Mrc1- and Rad9-mediated Rad53 activation.

(A, B) Precursor mass spectral scans of the unlabeled (light) and spiked-in SILAC-labeled (heavy) Rad53 and the co-precipitated Mrc1 (A) and Rad9 (B) tryptic fragment counterparts in the indicated strains. Spectra in (a) are from an unmodified Rad53 fragment as input control, and the others are from several phosphorylated Mrc1 or Rad9 fragments as indicated. The * in (A) indicates the m/z from contaminated peptide ions.

(C) Bar graphs showing the effects of SCD1, *rad9*, and *mrc1* mutations on phosphorylation levels of DNA damage inducible auto-phosphorylation sites after 45 min (a) and 135 min (b) treatment of MMS in S phase.

(D) Western blot analysis of Rad53 immunoprecipitations probed for Rad53 and co-precipitated Rad9. Samples were collected during alpha-factor G1-arrest (0') and at the indicated time points after release into the S phase with 0.05% MMS.

Figure S4. Combined effects of *rad9*Δ or *mrc1*Δ with SCD1 mutations on Rad53 auto-activating and priming phosphorylation.

(A) Precursor mass spectral scans for an unmodified Rad53$^{670\text{-}679}$ fragment FLLQDGEDIK and the phosphorylated Rad53$^{345\text{-}368}$ fragment VQGNGSFMKTFCGTLAYVAPEVIR (the underlined M352 and T354 was S-oxidized and phosphorylated, respectively) in the indicated, unlabeled "light" (L1~L11) experimental samples relative to the SILAC-labeled "heavy" (H) DNA-damaged WT references. The effects of SCD1 mutations with fewer TQ preserved (L1~L4) and the combined effects with *rad9*Δ (L5~L8) or *mrc1*Δ (L9~L11) on the levels of pT354 are shown in (a) to (c), respectively. Mass to charge ratio (m/z) of the monoisotopic precursor is labeled at each top panel.

(B and C) Monoisotopic peak XICs (with 25 ppm tolerance) for an unmodified Rad53$^{670\text{-}679}$ fragment (a) and the mono-phosphorylated rad53-T8-3AQ$^{1\text{-}17}$ fragment (b) in the indicated, unlabeled "Light" Rad53$^{T8\text{-}3AQ}$ relative to the normalized spiked-in "Heavy" DNA-damaged WT references. The effect of *rad9*Δ (B) or *mrc1*Δ (C) on the levels of mono-phosphorylated MENIAQPTQQSAQAAQR in *rad53-T8-3AQ* were semi-quantitated by normalizing the levels of the corresponding spiked-in references and their inputs. In panel b, the XICs of light

rad53-T8-3AQ$^{1-17}$ are principally from T8-mono-phosphorylated MENIAQPTQQSAQAAQR based on the tandem MS spectra (data not show), while the XICs of heavy Rad53$^{1-17}$ (MENITQPTQQSTQATQR) are from the mixture of four possible mono-phosphorylations at T5, T8, T12, and T15. The XICs in (C) were acquired from UHPLC-MS/MS analyses, thereby showing higher separation power than those in (B).

(D) Monoisotopic peak XICs (with 25 ppm tolerance) for an unmodified Rad53$^{670-679}$ fragment (a) and the mono- and di-phosphorylated SCD1 rad53-T5T8-2AQ$^{1-17}$ fragment (b and c, respectively) in the indicated, unlabeled "Light" Rad53$^{T5T8-2AQ}$ relative to the normalized spiked-in "Heavy" DNA-damaged WT references. The effect of *rad9*Δ (L2 relative to L1) or *mrc1*Δ (L3 relative to L1) on the levels of mono- and di-phosphorylated MENITQPTQQSAQAAQR in *rad53-T5T8-2AQ* were semi-quantitated by normalizing the levels of the corresponding spiked-in references and their inputs. In panels b and c, the XICs of heavy Rad53$^{1-17}$ (MENITQPTQQSTQATQR) are from the respective mixtures of four possible mono-phosphorylation and six possible di-phosphorylation at T5, T8, T12, and T15 within the SCD1 (see Table S2).

(E) Monoisotopic peak XICs (with 25 ppm tolerance) for an unmodified Rad53$^{670-679}$ fragment (a) and the mono-phosphorylated Rad53$^{1-17}$ fragment (b) in the unlabeled, indicated "Light" Rad53 relative to the normalized spiked-in "Heavy" DNA-damaged WT references.

Figure S5. Combined effects of *rad9*Δ with FHA mutations on phosphorylation dependent depletion of unphosphorylated SCD1 fragment. Monoisotopic peak XICs (with 25 ppm tolerance) for an unmodified Rad53$^{670-679}$ fragment (a) and the unphosphorylated Rad53$^{1-17}$ fragment (b) in the indicated, unlabeled "Light" strains relative to the normalized spiked-in

"Heavy" DNA-damaged WT references. Note that the L1 peaks were from the immuno-purified Rad53 WT in unperturbed S phase condition, while L2 to L4 peaks were from 0.05% MMS damaged S phase for WT, *rad53-R70A rad9*Δ, and *rad53-R605A rad9*Δ, respectively.

Supplementary Table 1. Genotypes of yeast strains used in this study.

Strain	Genotype	Source
W1588-4C	*MAT**a** ade2-1 can1-100 leu2-3,112 his3-11,15 trp1-1 ura3-1 RAD5*	R. Rothstein
2159-9D	*MAT**α** ADE2 CAN1 mrc1-AQ-13myc-HIS3*	H. Klein
Y53	*sml1::HIS3*	(1)
Y57	*rad53-R70A sml1::HIS3*	(2)
Y59	*rad53-K227A sml1::HIS3*	(2)
Y122	*rad9::LEU2 sml1::HIS3*	(3)
Y123	*rad9::LEU2 rad53-R70A sml1::HIS3*	(3)
Y205	*rad53-R605A sml1::HIS3*	(4)
Y206	*rad53-R70A-R605A sml1::HIS3*	(4)
Y1015	*rad53-4AQ sml1::HIS3*	(5)
Y1016	*rad53-T5-3AQ sml1::HIS3*	(5)
Y1017	*rad53-T8-3AQ sml1::HIS3*	(5)
Y1018	*rad53-T5T8-2AQ sml1::HIS3*	(5)
Y1075	*rad9::LEU2 rad53-R605A sml1::HIS3*	This study
Y1095	*rad9::LEU2 rad53-R70A-R605A sml1::HIS3*	This study
Y1206	*rad9::LEU2 rad53-4AQ sml1::HIS3*	This study
Y1208	*rad9::LEU2 rad53-T5-3AQ sml1::HIS3*	This study
Y1210	*rad9::LEU2 rad53-T8-3AQ sml1::HIS3*	This study
Y1212	*rad9::LEU2 rad53-T5T8-2AQ sml1::HIS3*	This study
Y1378	*mrc1-AQ-13myc-HIS3 rad53-4AQ sml1::HIS3*	This study
Y1397	*rad53-T5T8T15-1AQ sml1::HIS3*	This study
Y1398	*rad53-T5T8T12-1AQ sml1::HIS3*	This study
Y1451	*rad9::LEU2 rad53-T5T8T15-1AQ sml1::HIS3*	This study
Y1456	*rad9::LEU2 rad53-T5T8T12-1AQ sml1::HIS3*	This study

Y1584	*lys2::NAT arg4::KAN CAN1*	This study
Y1587	*rad53-D339A sml1::HIS3*	This study
Y1632	*mrc1-AQ-13myc-HIS3 sml1::HIS3*	This study
Y1633	*mrc1-AQ-13myc-HIS3 rad9::LEU2 sml1::HIS3*	This study
Y1634	*mrc1-AQ-13myc-HIS3 rad9::LEU2 rad53-4AQ sml1::HIS3*	This study

References:

1. Zhao, X., Muller, E. G. D., and Rothstein, R. (1998) A Suppressor of Two Essential Checkpoint Genes Identifies a Novel Protein that Negatively Affects dNTP Pools. *Molecular Cell* 2, 329-340

2. Pike, B. L., Hammet, A., and Heierhorst, J. (2001) Role of the N-terminal Forkhead-associated Domain in the Cell Cycle Checkpoint Function of the Rad53 Kinase. *Journal of Biological Chemistry* 276, 14019-14026

3. Pike, B. L., Yongkiettrakul, S., Tsai, M.-D., and Heierhorst, J. (2003) Diverse but Overlapping Functions of the Two Forkhead-associated (FHA) Domains in Rad53 Checkpoint Kinase Activation. *J. Biol. Chem.* 278, 30421-30424

4. Pike, B. L., Tenis, N., and Heierhorst, J. (2004) Rad53 Kinase Activation-independent Replication Checkpoint Function of the N-terminal Forkhead-associated (FHA1) Domain. *J. Biol. Chem.* 279, 39636-39644

5. Lee, H., Yuan, C., Hammet, A., Mahajan, A., Chen, E. S., Wu, M. R., Su, M. I., Heierhorst, J., and Tsai, M. D. (2008) Diphosphothreonine-specific interaction between an SQ/TQ cluster and an FHA domain in the Rad53-Dun1 kinase cascade. *Mol Cell* 30, 767-778

Chen_Fig. S1

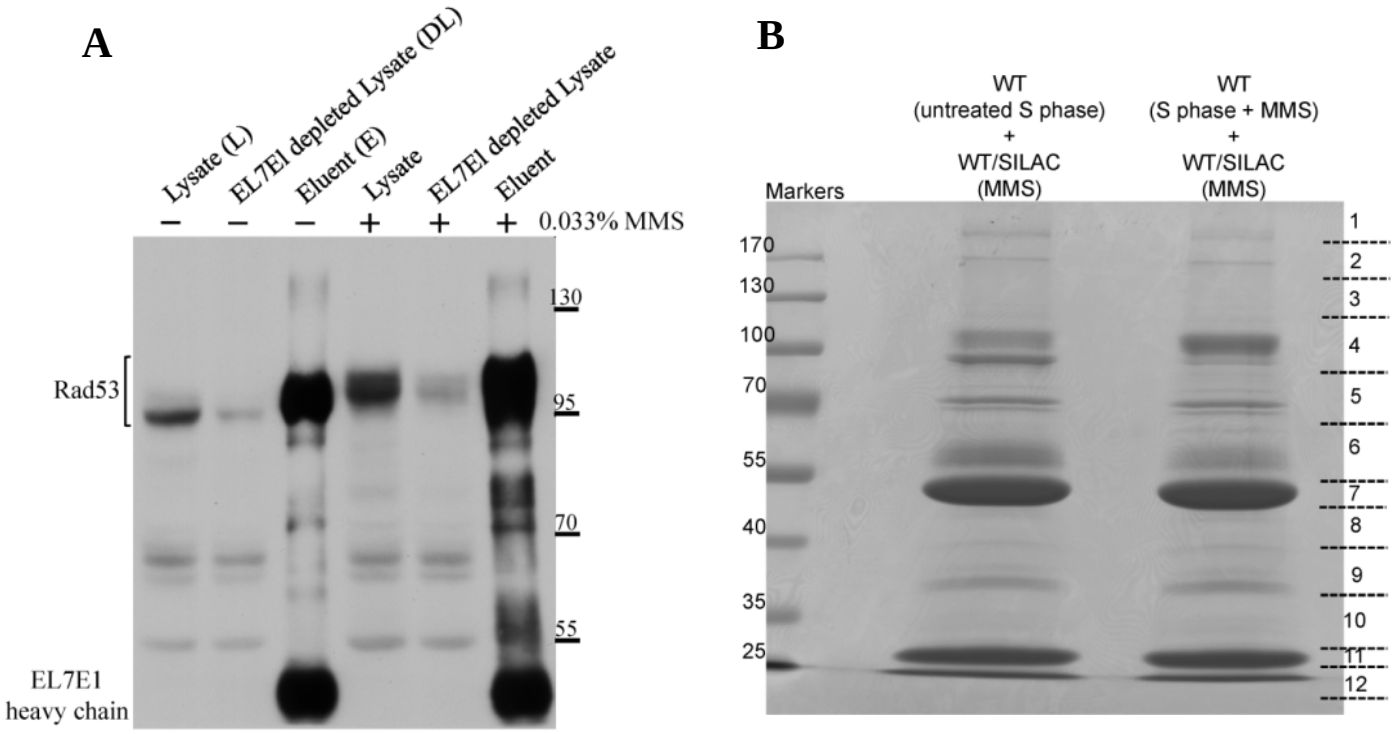
A
Lysate (L)
EL7E1 depleted Lysate (DL)
Eluent (E)
Lysate
EL7E1 depleted Lysate
Eluent
− − − + + + 0.033% MMS
Rad53
EL7E1
heavy chain
130
95
70
55
B
Markers
WT
(untreated S phase)
+
WT/SILAC
(MMS)
WT
(S phase + MMS)
+
WT/SILAC
(MMS)
170
130
100
70
55
40
35
25
1
2
3
4
5
6
7
8
9
10
11
12

Chen_Fig. S2

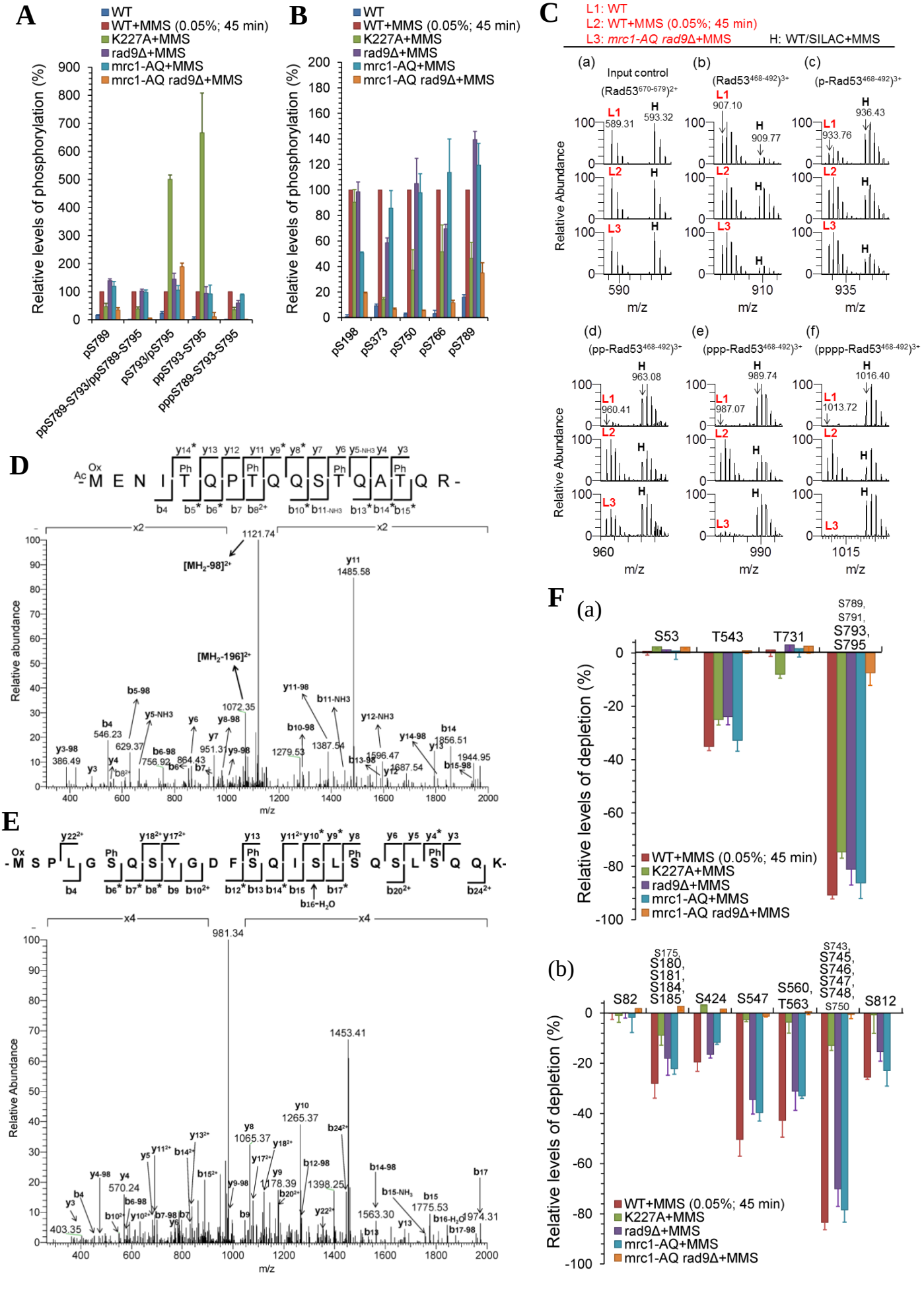
A
WT
WT+MMS (0.05%; 45 min)
K227A+MMS
rad9Δ+MMS
mrc1-AQ+MMS
mrc1-AQ rad9Δ+MMS
Relative levels of phosphorylation (%)
pS789
ppS789-S793/ppS789-S795
pS793/pS795
ppS793-S795
pppS789-S793-S795
B
pS198
pS373
pS750
pS766
pS789
C
L1: WT
L2: WT+MMS (0.05%; 45 min)
L3: mrc1-AQ rad9Δ+MMS
H: WT/SILAC+MMS
Input control
(Rad53670-679)2+
(Rad53468-492)3+
(p-Rad53468-492)3+
(pp-Rad53468-492)3+
(ppp-Rad53468-492)3+
(pppp-Rad53468-492)3+
Relative Abundance
m/z
D
Ac-M E N I T Q P T Q Q S T Q A T Q R-
Ox
Ph
[MH2-98]2+
[MH2-196]2+
Relative abundance
m/z
E
-M S P L G S Q S Y G D F S Q I S L S Q S L S Q Q K-
b16-H2O
Relative Abundance
m/z
F
(a)
S53
T543
T731
S789, S791, S793, S795
Relative levels of depletion (%)
WT+MMS (0.05%; 45 min)
K227A+MMS
rad9Δ+MMS
mrc1-AQ+MMS
mrc1-AQ rad9Δ+MMS
(b)
S82
S175, S180, S181, S184, S185
S424
S547
S560, T563
S743, S745, S746, S747, S748, S750
S812

A

L1: WT+MMS (0.05%; 45min), L2: rad53-4AQ+MMS, L3: rad9Δ+MMS, L4: rad53-4AQ rad9Δ+MMS, H:WT/SILAC+MMS

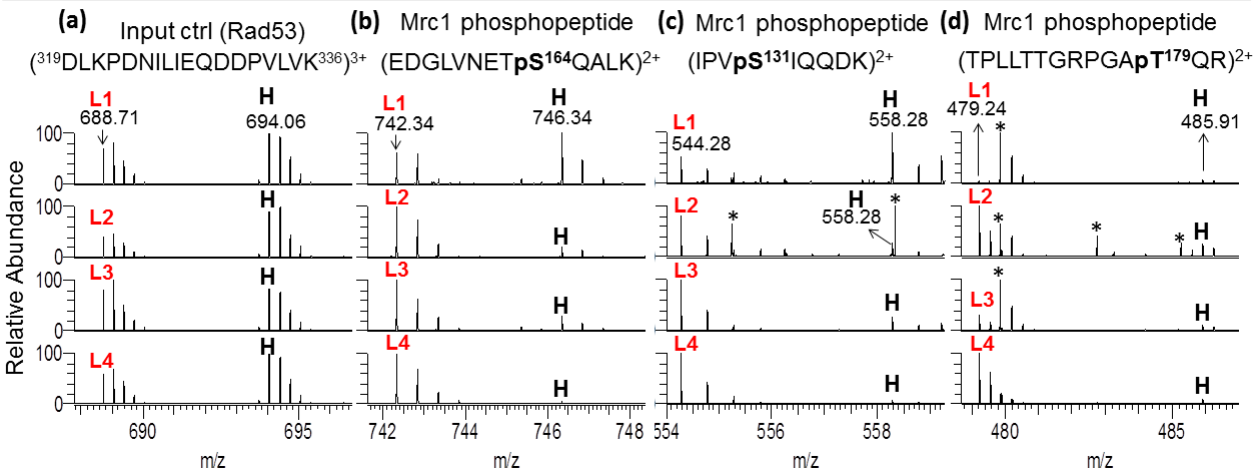

B

L1: WT+MMS (0.05%; 45 min), L2: rad53-4AQ+MMS, L3: mrc1-AQ+MMS, L4: rad53-4AQ mrc1-AQ+MMS
H: WT/SILAC+MMS

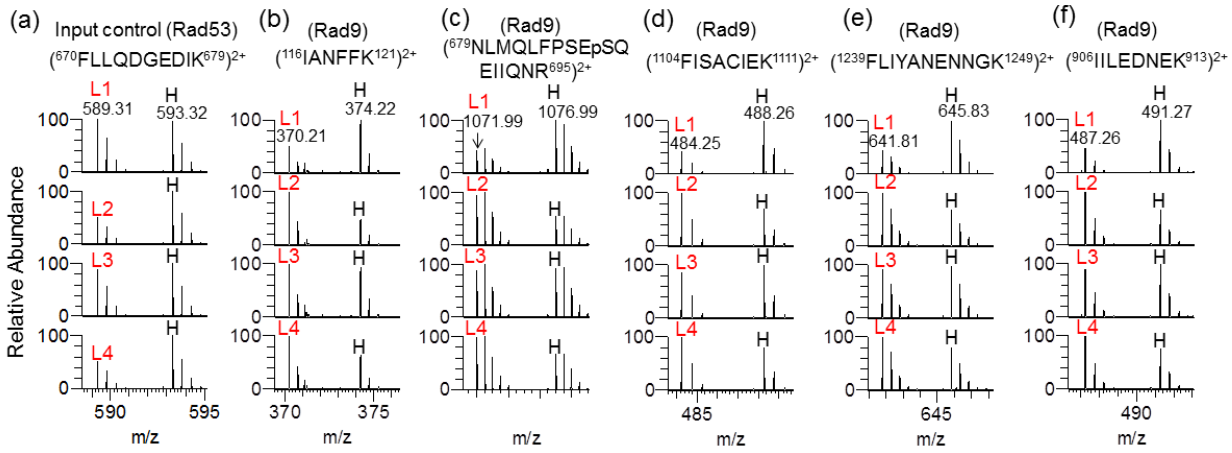

C

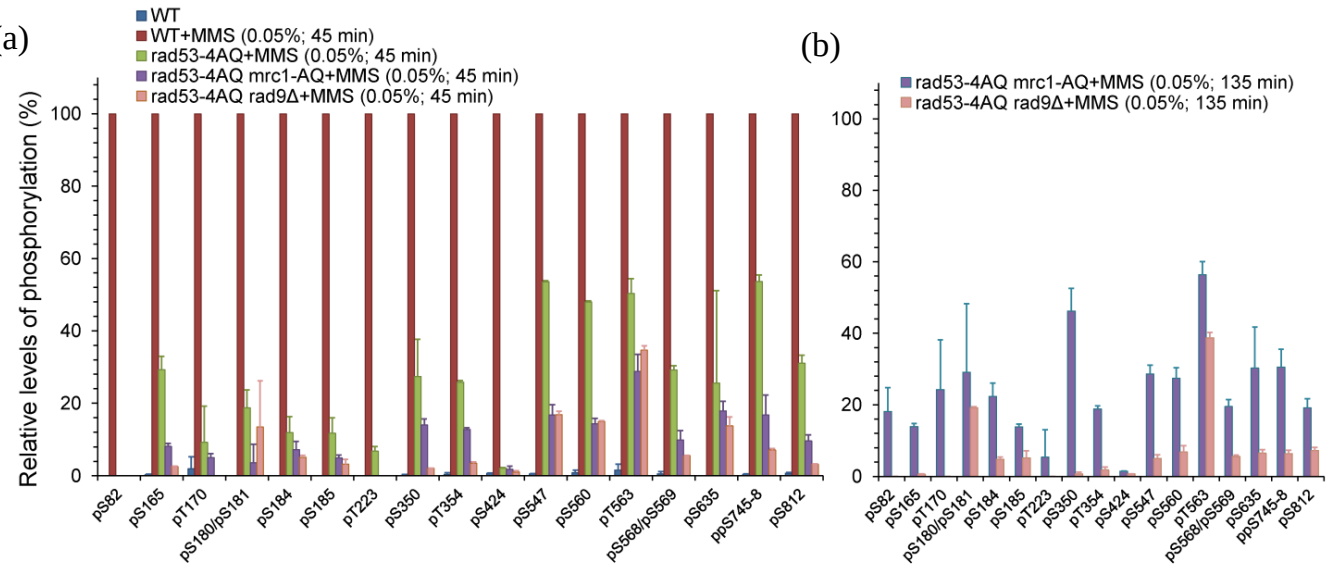

D

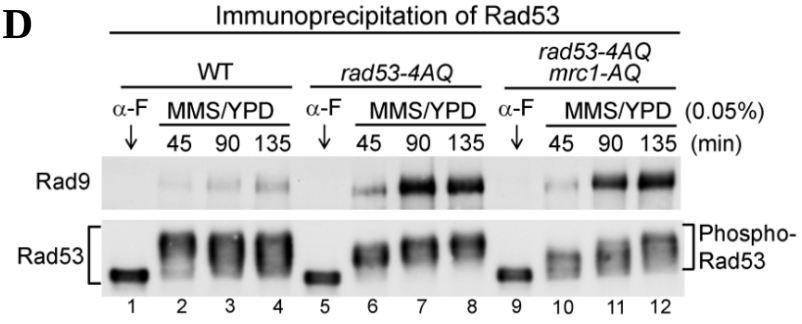

Chen_Fig. S4

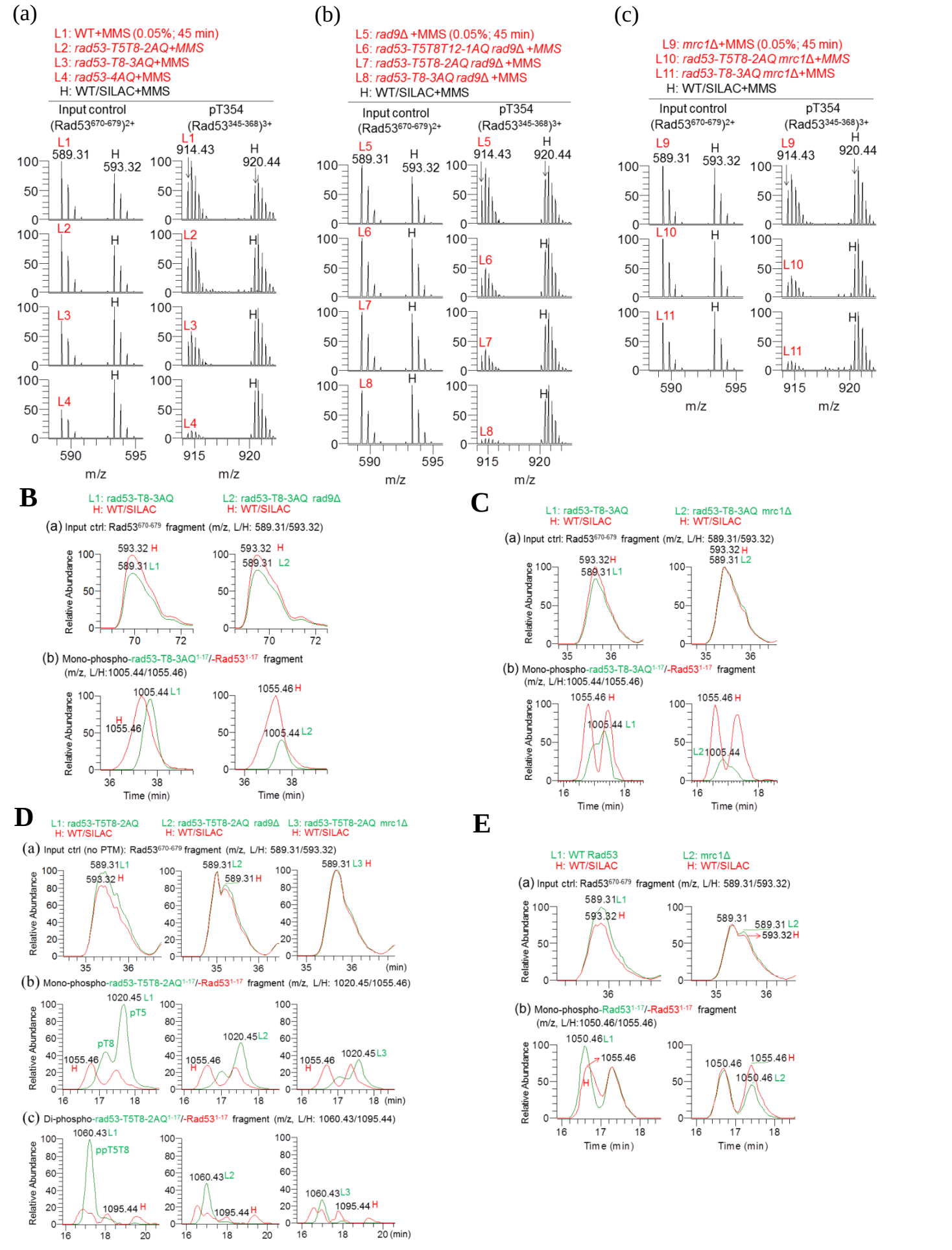
A
(a)
L1: WT+MMS (0.05%; 45 min)
L2: rad53-T5T8-2AQ+MMS
L3: rad53-T8-3AQ+MMS
L4: rad53-4AQ+MMS
H: WT/SILAC+MMS
Input control (Rad53670-679)2+
pT354 (Rad53345-368)3+
(b)
L5: rad9Δ +MMS (0.05%; 45 min)
L6: rad53-T5T8T12-1AQ rad9Δ +MMS
L7: rad53-T5T8-2AQ rad9Δ +MMS
L8: rad53-T8-3AQ rad9Δ +MMS
H: WT/SILAC+MMS
(c)
L9: mrc1Δ+MMS (0.05%; 45 min)
L10: rad53-T5T8-2AQ mrc1Δ+MMS
L11: rad53-T8-3AQ mrc1Δ+MMS
H: WT/SILAC+MMS
m/z
B
L1: rad53-T8-3AQ H: WT/SILAC
L2: rad53-T8-3AQ rad9Δ H: WT/SILAC
(a) Input ctrl: Rad53670-679 fragment (m/z, L/H: 589.31/593.32)
(b) Mono-phospho-rad53-T8-3AQ1-17/-Rad531-17 fragment (m/z, L/H:1005.44/1055.46)
Relative Abundance
Time (min)
C
L1: rad53-T8-3AQ H: WT/SILAC
L2: rad53-T8-3AQ mrc1Δ H: WT/SILAC
(a) Input ctrl: Rad53670-679 fragment (m/z, L/H: 589.31/593.32)
(b) Mono-phospho-rad53-T8-3AQ1-17/-Rad531-17 fragment (m/z, L/H:1005.44/1055.46)
Relative Abundance
Time (min)
D
L1: rad53-T5T8-2AQ H: WT/SILAC
L2: rad53-T5T8-2AQ rad9Δ H: WT/SILAC
L3: rad53-T5T8-2AQ mrc1Δ H: WT/SILAC
(a) Input ctrl (no PTM): Rad53670-679 fragment (m/z, L/H: 589.31/593.32)
(b) Mono-phospho-rad53-T5T8-2AQ1-17/-Rad531-17 fragment (m/z, L/H: 1020.45/1055.46)
(c) Di-phospho-rad53-T5T8-2AQ1-17/-Rad531-17 fragment (m/z, L/H: 1060.43/1095.44)
Relative Abundance
(min)
E
L1: WT Rad53 H: WT/SILAC
L2: mrc1Δ H: WT/SILAC
(a) Input ctrl: Rad53670-679 fragment (m/z, L/H: 589.31/593.32)
(b) Mono-phospho-Rad531-17/-Rad531-17 fragment (m/z, L/H:1050.46/1055.46)
Relative Abundance
Time (min)

Chen_Fig. S5

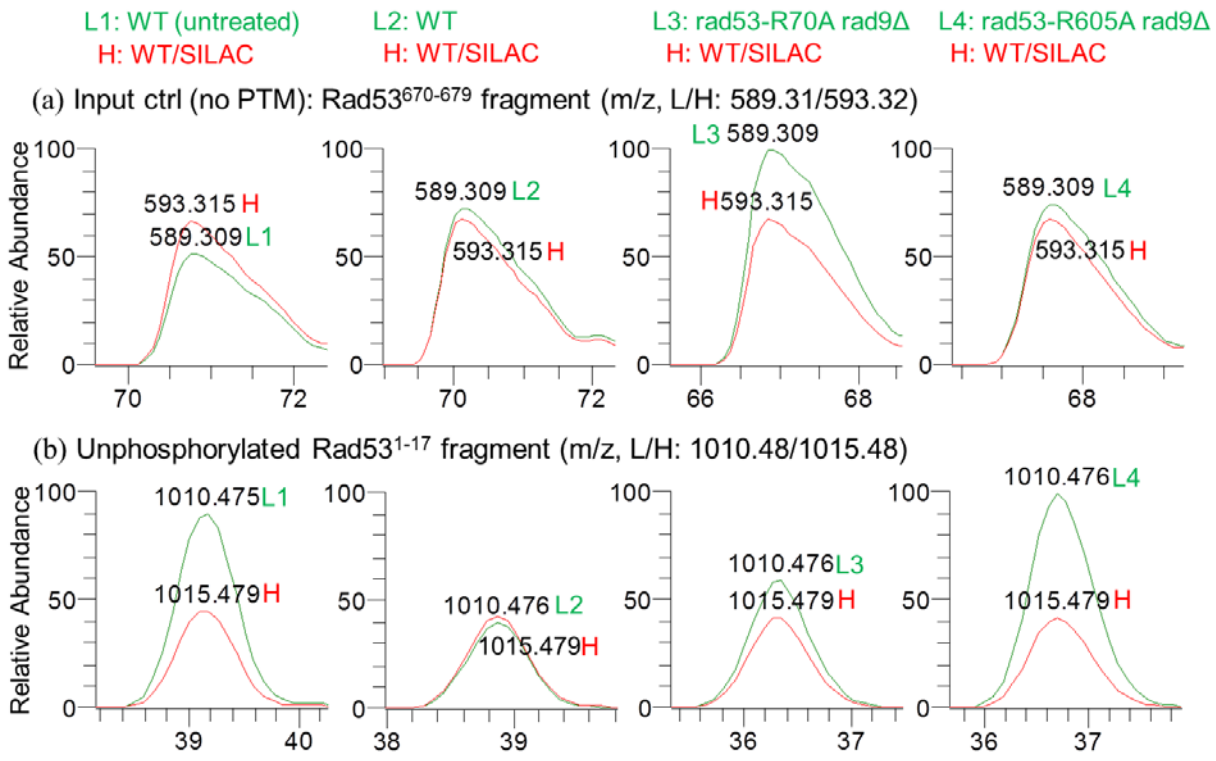
L1: WT (untreated)
H: WT/SILAC
L2: WT
H: WT/SILAC
L3: rad53-R70A rad9Δ
H: WT/SILAC
L4: rad53-R605A rad9Δ
H: WT/SILAC
(a) Input ctrl (no PTM): Rad53670-679 fragment (m/z, L/H: 589.31/593.32)
Relative Abundance
593.315 H
589.309 L1
589.309 L2
593.315 H
L3 589.309
H593.315
589.309 L4
593.315 H
(b) Unphosphorylated Rad531-17 fragment (m/z, L/H: 1010.48/1015.48)
1010.475 L1
1015.479 H
1010.476 L2
1015.479 H
1010.476 L3
1015.479 H
1010.476 L4
1015.479 H